



Titanium/FRP hybrid sandwich: in-plane flexural behaviour of short beam specimens

C. Bellini, V. Di Cocco, F. Iacoviello, L.P. Mocanu, L. Sorrentino

University of Cassino and Southern Lazio, Italy

costanzo.bellini@unicas.it, <http://orcid.org/0000-0003-4804-6588>

vittorio.dicocco@unicas.it, <http://orcid.org/0000-0002-1668-3729>

francesco.iacoviello@unicas.it, <http://orcid.org/0000-0002-9382-6092>

larisapatricia.mocanu@unicas.it, <https://orcid.org/0000-0002-3432-9774>

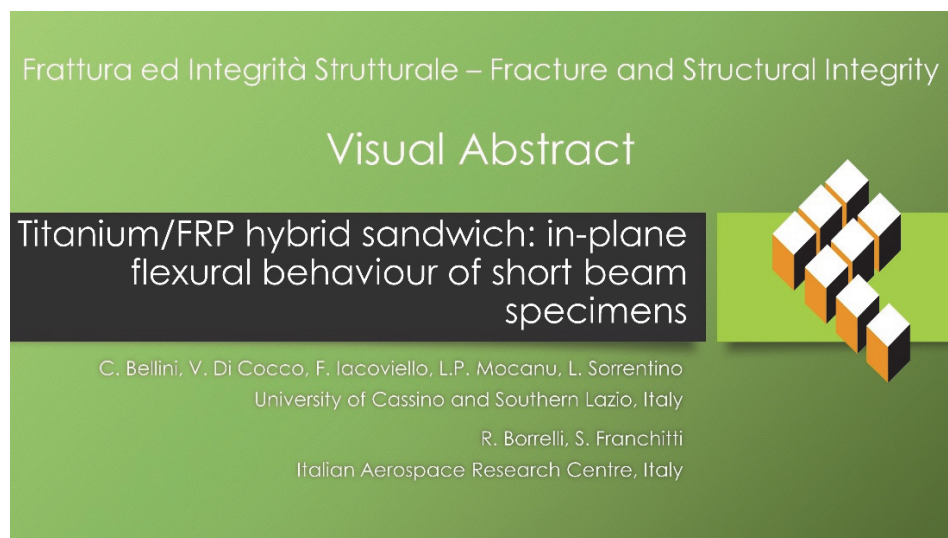
luca.sorrentino@unicas.it, <https://orcid.org/0000-0002-5278-7357>

R. Borrelli, S. Franchitti

Italian Aerospace Research Centre, Italy

r.borrelli@cira.it, <https://orcid.org/0000-0002-5848-5958>

s.franchitti@cira.it, <https://orcid.org/0000-0002-3064-1285>



Citation: Bellini, C., Borrelli, R., Di Cocco, V., Franchitti, S., Iacoviello, F., Mocanu, L.P., Sorrentino, L., Titanium/FRP hybrid sandwich: in-plane flexural behaviour of short beam specimens, *Frattura ed Integrità Strutturale*, 69 (2024) 18-28.

Received: 30.01.2024

Accepted: 03.04.2024

Published: 13.04.2024

Issue: 07.2024

Copyright: © 2024 This is an open access article under the terms of the CC-BY 4.0, which permits unrestricted use, distribution, and reproduction in any medium, provided the original author and source are credited.

KEYWORDS. Fibre reinforced polymer, Titanium, Electron Beam Melting, Sandwich beam, In-plane behaviour.



INTRODUCTION

The transportation sector is facing increased regulations regarding safety and pollutant emission, which can be addressed through the adoption of lightweight design solutions. To meet these requirements, innovative hybrid sandwich materials, which combine composite skins with a metal lattice core, are being developed. This approach offers benefits due to the high specific stiffness and strength of the two types of materials. It is important to emphasize that lattice structures must be considered as structurally homogeneous materials, although they might be considered as structures when studying the behaviour of individual cells [1]. Basically, the difference between lattice materials and structural frames lies in their dimensions; lattice structures typically operate on a scale ranging from microns to millimetres [2]. According to Bellini et al. [3], lattice materials consist of small beams systematically situated in the space, resulting in a new material with high specific mechanical properties. The lattice structures can be categorized based on the geometry of their cell which consists of the foundational set of beams forming the structure, as reported by Bellini et al. [4]. These structures, less common in the past due to production limitations, have gained new possibilities with the advent of additive manufacturing (AM) technology. Lattice structures are used in a variety of industries, such as aerospace, biomedical, aviation, and automotive. Various manufacturing methods can be used to fabricate lattice structures, from traditional processes such as machining, filament winding and casting, to advanced technologies such as additive manufacturing, including Electron Beam Melting (EBM), as discussed by Fan et al. [5], Bellini et al. [6], and Queheillalt et al. [7]. Dong et al. [8] have revealed that these techniques are increasingly reliable as well as capable of producing intricate geometric components. Furthermore, as noted by Razavi et al. [9] and Benedetti et al. [10], post-processing techniques are developed to mitigate material damage and part defects resulting from the production process.

The integration of composite and lattice materials into cored structures enhances specific mechanical performances, especially under bending stress conditions. Unlike traditional honeycomb structures commonly used for core production, the approach investigated in this work involves manufacturing lattice-cored structures with FRP (Fibre Reinforced Polymer) skins, which provides a comparatively simple processing method. Bellini et al. [11] pointed out that common honeycomb cores often necessitate intricate processes to achieve complex shapes, which can potentially compromise the integrity of the core. Conversely, lattice material can be manufactured directly into the desired final shape for the core, even in parts with complex geometries. Moreover, while honeycomb cores may experience deformation under the pressure required for the curing in an autoclave, lattice cores exhibit greater robustness.

Various research teams have investigated the mechanical properties of lattice structures fabricated by using AM processes, and their results have been documented in several publications. In a study by Leary et al. [12], different lattice structures were created by manipulating geometrical parameters like beam diameter and cell type to identify possible manufacturing limits. In addition, the team carried out experiments to evaluate the mechanical properties of the manufactured specimens. Lampeas et al. [13] developed a numerical model for simulating additive manufacturing processes, aiming to explore the relationship between failure mechanisms and process variables. Epasto et al. [14] conducted mechanical tests on lattice structures with varying unit cell sizes, revealing that larger cell sizes led to inferior mechanical behaviour. Liu et al. [15] utilized X-ray computed tomography to examine process-induced defects in a lattice structure and determined the structures' mechanical behaviour. In this manner, they were able to link the flaws to the causes of failure. Mahbod and Asgari [16] designed lattice structures with functionally graded porosity, aiming to enhance the mechanical response to crushing loads. Cantaboni et al. [17] found a strong effect of the cell orientation with respect to the building direction and the specimens on the mechanical properties of lattice structures made of Co-Cr-Mo alloy, and the mechanical behaviour could be further influenced by heat treatment. Magarò et al. [18] investigated the changes in the local mechanical properties of the beams belonging to stainless steel lattice structures. In such a manner, they were able to improve the accuracy of the FEM model used for the mechanical simulation of such structures. Carraturo et al. [19] enhanced the precision of the FEM model by adopting the real geometry of the specimen instead of the nominal one. In fact, due to the small size of the beams, un-neglectable differences may arise between the two geometries. A discrepancy between nominal and produced geometry was also found by Bellini et al. [20], who produced and measured several thin beams, varying the building orientation and the part diameter. The effects of the geometrical discrepancy were studied by Di Caprio et al. [21] too, who proposed a new methodology for assessing the errors induced by this issue on the numerical modelling of such structures. Fiorentin et al. [22] investigated the effect of the process-induced residual stresses on the fatigue characteristics of a topologically-optimized part, utilizing a FEM model to simulate the manufacturing process and evaluate the influence of building direction. Taghipoor and Nouri [23] studied the effect of the cell characteristics of lattice structures made of expanded metal sheets by using a numerical model, and they discovered that the cell orientation was a critical parameter. Zargarian et al. [24] proposed a numerical model to analyse the effect of various factors, including the relative density and the bulk material fatigue properties, on the high cycle fatigue behaviour of lattice structures.

The main goal of the present analysis is to assess the influence of skin materials on the flexural characteristics of sandwich specimens made with FRP (Fiber Reinforced Polymer) skins and metal cores produced through AM. In addition, sandwich specimens with titanium skin and core were produced and tested for comparison purposes. While numerous papers compare the mechanical behaviour of various types of bulk FRP laminates, such as those by Figlus et al. [25] and Koziol [26], only few studies specifically addressed hybrid cored structures [27,28]. Flexural load, commonly encountered in structural components of vehicles, has typically been examined in the out-of-plane direction, parallel to the thickness of the skins. On the other hand, the perpendicular direction, or in-plane load arrangement, has received limited attention. In this study, particular focus was given on this latter setup, employing short beam specimens for analysis.

The structure of the present work includes several sections. After the introduction part, the first section "Materials and Methods" introduces the case study, defining the characteristics of the samples to be evaluated, including size, shape, and composition (titanium and fibre composites). Next, the manufacturing process is explained. Depending on the skin type, two possible methods were used: i) the all-titanium specimens were manufactured in a single step, with the lattice core and skins printed together; ii) FRP skin specimens were subjected to a two-step technique: initially, the EBM process was used to create the cores, followed by the placement of prepreg sheets on the top of the cores, which were then autoclaved for co-cure. After that, experimental three-point bending load tests were conducted to test the fabricated specimens, and the fracture surfaces were analysed to delineate the fracture mechanisms. The results were reported and discussed in the "Results" section. Finally, the conclusions were summarised in the last section.

MATERIALS AND METHODS

The present study uses the three-point bending test to assess the short-beam bending characteristics of different sandwich specimens. The main difference among the different samples investigated is the material used for the skins, including CFRP, AFRP, or titanium. Specifically, two different types of carbon fibres are used for CFRP. All specimens had a titanium core, and a short beam geometry is chosen for the flexural loading test.

The beam core was composed of octet-truss cells, known for its great mechanical properties and wide application. This cell consisted of two lattice solids: an inner octahedron and an outer cube with centred faces. Each cell, with an edge of 6 mm, contained 36 trusses of 1 mm in diameter. The sample core had a section measuring 10x9 mm² and a length of 30 mm. Skin thickness remained constant at 1 mm for all types. Maintaining this uniformity was essential to conduct significant comparisons between skin types. The geometry of the sample is shown in Fig. 1. The lattice was built using Ti6Al4V alloy powder as the raw material, which is specifically adapted to the EBM process, and is produced by atomization. The skins were realized with different materials, depending on the specimen type: the same powder as the core was used for the all-titanium specimens, while for the CFRP and AFRP specimens, a carbon or aramid prepreg was used. It is important to note that the aramid based prepreg had a reinforcement fabric with a satin weave style, while the two carbon prepreps had either a plain weave (PW) or a twill weave (TW) style. The former was suitable for general purposes, while the latter was more specific for structural applications. The mechanical properties of the used materials are reported in Tab. 1. To ensure a robust connection between the titanium lattice and the composite material skin, a structural adhesive was employed, specifically the Hexcel Hexbond ST 1035 epoxy adhesive in film form. However, the adhesive was not necessary for the all-titanium specimens, since the skins were printed at the same time as the lattice core.

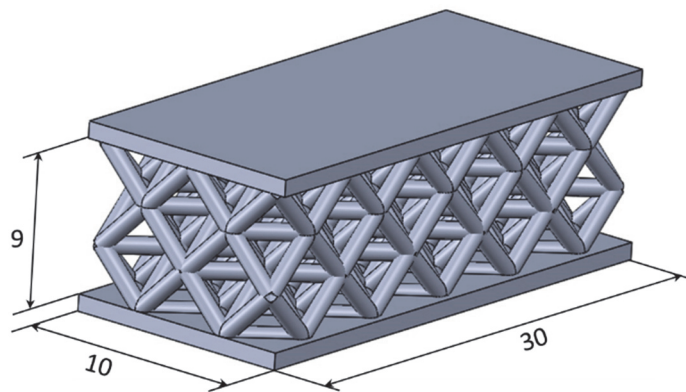


Figure 1: Geometrical characteristic of the short beam hybrid specimen.



Material	Density [kg/m ³]	Young's modulus MPa	Tensile strength MPa
Ti6Al4V powder	4400	104800	900
PW Carbon	1540	50000	650
TW Carbon	1461	65000	800
Aramid composite	1350	30000	524

Table 1: Properties for all the materials involved in the study.

Different manufacturing processes were used to produce the samples, depending on the skin material. While the lattice core for all samples was created using EBM technology, chosen for its prevalence in the aerospace industry, differences emerged in the production of the skin. The titanium samples were produced using additive manufacturing, with the skin printed at the same time as the lattice core. While, in the other cases, composite skins were added by co-curing, in which the prepreg and adhesive were cured together using the core as a sort of mould. Summarizing, titanium skin samples underwent a single-step process, while FRP samples followed a two-step process.

In the production of parts with both cores and skins made of titanium, the initial step involved the design of a digital geometric model of the core. Materialise Magics software, which is suitable for modelling lattice structures within a limited volume, was used for this purpose. Once the CAD (Computer Aided Design) model was completed, it was imported into Materialise Magics for design optimization. Configuration of the slices and process themes was then performed with ARCAM Build Processor and EBM control 3.2, respectively. For titanium skinned samples, the CAD of the skins was integrated with that of the core before slicing, allowing an interpenetration of the digital models of 0.2 mm to ensure proper joining of the parts. This approach facilitated the use of different process parameter sets for the skin and the core with themes suitable for bulk and lattice parts, respectively. Then, the actual manufacturing process commenced by setting up the ARCAM A2X EBM system, and the hoppers were loaded with titanium powder. To ensure optimal conditions, the production chamber vacuum was established prior to electron beam calibration, followed by preheating the building plate. Once the preheating temperature (approximately 700 °C) was achieved, specimen cores were produced following the procedure typical of an additive manufacturing process based on a powder bed. At the end of the production process, the chamber was gradually cooled to room temperature, and the samples were carefully extracted from the unmelted powder mass. Subsequently, a complete cleaning process started using sandblasting equipment and a pressurized air chamber known as the Powder Recovery System. In addition, an ultrasonic bath was used for complete cleaning.

The FRP samples required a two-step manufacturing procedure, necessary for the addition of laminate skins. The core of the samples was produced through EBM, as described before, while for the fabrication of the composite skins, the prepreg-vacuum bag technique was chosen. The FRP prepreg plies and the produced lattice core were assembled on the metal mould. To ensure consistency, it was decided to use five prepreg plies for carbon skins and four for aramid skins, achieving a uniform thickness of approximately 1 mm for all face sheets. This uniformity was crucial for making meaningful comparisons among the different types of specimens. Before using the vacuum bag to seal the mould, all layered specimens were first covered with the release film and the breather fabric, a common procedure in the vacuum bag process. After sealing, the mould was placed in the autoclave for the curing step. Once the thermal cycle was completed, the bag was removed from the autoclave and the specimens were extracted. Next, the resin burrs were removed, and the specimens were ready for testing.

The manufactured specimens, as shown in Fig. 2, were tested using the three-point bending setup: placed on two supports, each specimen was centrally loaded by a loading nose. Although this method is commonly applied to sandwich structures, it generally focuses on determining out-of-plane properties. However, as previously mentioned, this study specifically investigates in-plane attributes. Therefore, the load was applied along the skin direction, as illustrated in Fig. 3. The span length, defined as the distance between the supports, was set at 20 mm, and the loading rate was maintained at 2 mm/min. Loading was prosecuted until each specimen fractured. Five samples were tested for each type of specimen, for a total of 20 experimental runs.

At the end of the bending test, the specimens were analysed using an optical microscope to delineate the damage mechanisms occurring during the loading. The optical microscope used for this purpose was the Nikon SMZ800.



Figure 2: Titanium, AFRP and PW-CFRP short beam hybrid specimens, from left to right.

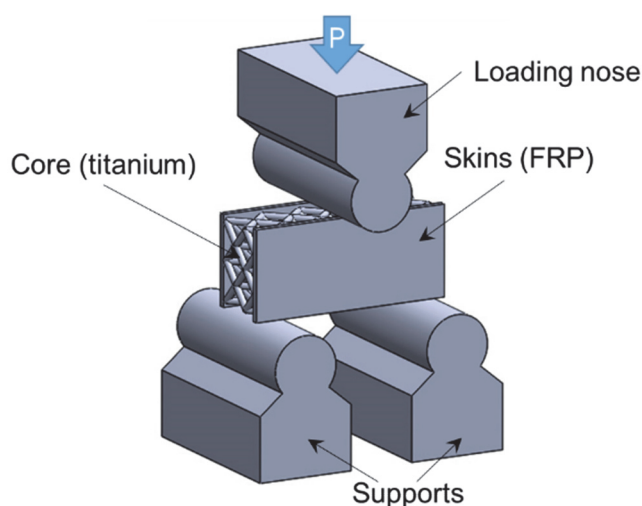


Figure 3: In-plane three-point bending test.

RESULTS

The load-displacement curves of all the short beam specimens subjected to three-point bending tests are shown in Fig. 4. For each specimen type, one curve, relevant to a single sample, is represented in the graph to improve clarity and readability. This simplification is justified by the acceptable standard deviation of the experimental data relevant to the same specimen type, which was below 10%. In particular, the titanium specimens presented the highest strength, reaching a maximum load of 7449 N. In contrast, the PW carbon and the aramid specimens showed the lowest strength, reaching maximum loads of 3993 N and 4125 N, respectively. The TW carbon specimens exhibited slightly higher strength, with a maximum load of 4604 N. Although the titanium skinned specimens presented the highest strength, they underwent the least deformation before load drop, with a displacement of 1.1 mm. On the contrary, the TW carbon samples showed the highest deformation of 2 mm, almost twice as much as the all-titanium ones. The PW carbon and the aramid samples recorded a displacement of 1.7 mm for both types.

Regarding the shape of the load-displacement curves, the titanium-skinned samples showed a linear increase in load up to 5700 N, followed by a non-linear trend leading to the maximum value, with no minor load drops. After, there was a main load drop, which quickly reduced the load to a neglectable value, indicating minimal residual strength after the main failure event. In contrast, the FRP specimens showed a similar trend as the all-titanium one, although with slight variations. The initial phase of load increase in the curves was characterized by a linear trend followed by a minor load drop, probably associated with the failure of some fibres in the composite skins. The subsequent section exhibited a non-linear load increase with additional load drops, indicating the successive breakage of more fibres in both CFRP and AFRP specimens. Then,

after reaching the maximum load, there was a drop in load. After this main drop, there was a decrease in load influenced by the skin material: the AFRP specimens exhibited a plateau between 2500 and 2000 N, while the TW carbon and PW carbon specimens showed a plateau around 1000 N. This denoted a higher residual resistance in the AFRP specimens compared to the CFRP ones, probably due to the different failure modes, as it will be explained later in the text.

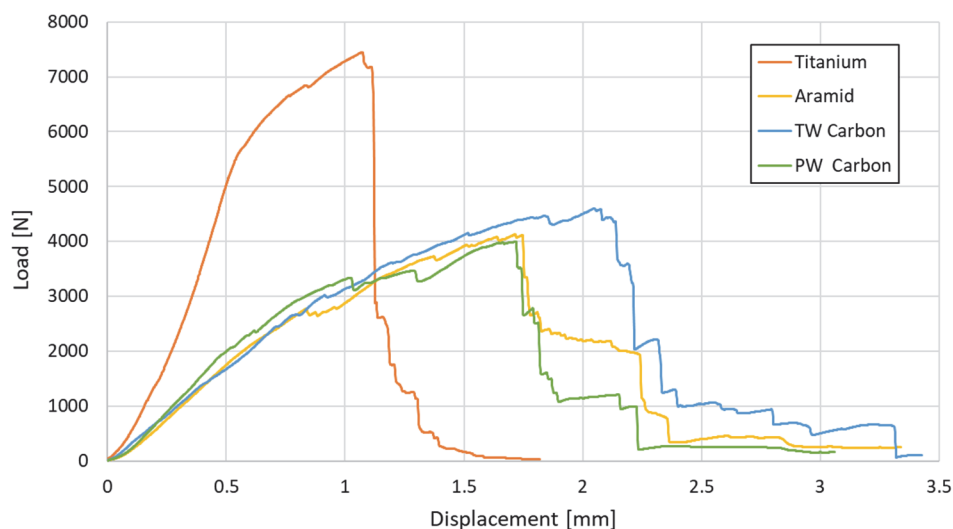


Figure 4: Load displacement curves recorded from in-plane three-point bending tests.

In the transport field, materials must possess properties of stiffness, strength, and lightness. To facilitate the meaningful comparison of the capacity and efficiency among the different specimens considered in this work, a new parameter, the PI (Performance Index), was introduced and calculated for all the cases analysed. This parameter was defined as the ratio between the maximum load attained and the weight of the relevant specimen. As shown in Tab. 2, the titanium skinned specimens were the heaviest, with an average weight of 5 g. The weights of all the FRP specimens were almost similar ranging between 3.2 and 3.3 g, an expected result due to the similar size of the specimens and the different density of the constituent materials, with titanium having the highest density. The table also reveals that the titanium specimen had the highest performance index, while the PW carbon specimens had the lowest. Despite the maximum load achieved the PW carbon specimens was only slightly different from that of the aramid specimens, the lower density of aramid resulted in a lower weight, justifying the greater difference in performance index.

Skin type	Weight [g]	Max load [N]	PI [N/g]
Titanium	5.00	7449	1489
Aramid	3.17	4126	1300
TW Carbon	3.24	4605	1421
PW Carbon	3.29	3993	1215

Table 2: Performance indexes calculated for the studied types of hybrid samples.

Micrographs of the fracture zone were acquired to further investigate the fracture mechanism. Observing the micrographs in Fig. 5 for the all-titanium specimens, it is evident that the surface finish of the skins resembles that of an EBMed part. The surface had considerable roughness, probably due to partially melted powder particles on the surface. The mark left by the loading nose was noticeably evident on the upper surface, more so than on other types of specimens. This difference was reflected in the appearance of the load-displacement curves depicted in Fig. 4, where the tip region at the beginning of the curves is more pronounced for the all-titanium specimens. The crack started from the bottom of the short beam, positioned in the centre of the specimen, and propagated toward the top surface. The crack advanced along the boundaries of the partially melted particles, without splitting them. Moreover, the fracture surface was not perpendicular to the skin

surface and had a quite rough appearance, typical of a ductile fracture. This ductile behaviour of this material was found also in previous studies [4].

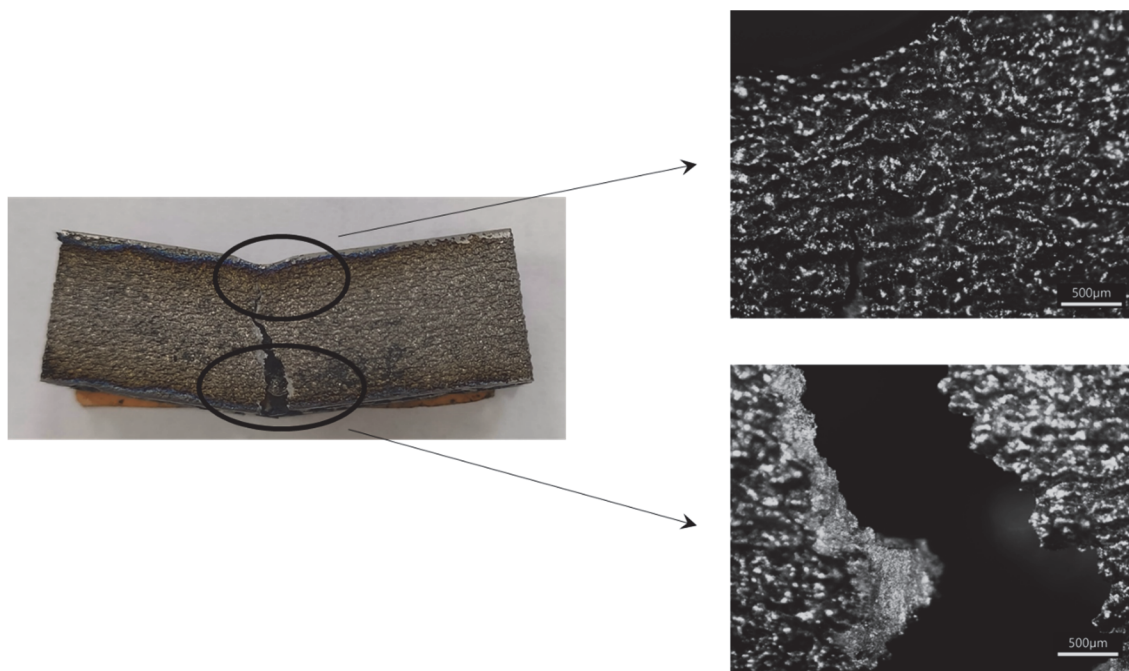


Figure 5: Titanium-skin fractured specimen.

The failure surfaces of the TW and PW carbon specimens can be observed in Figs. 6 and 7, respectively. There is a noticeable difference in the surface appearance of these two types of specimens: in the former, the carbon fibres are more prominent, indicating a higher resin content in the skins than in the latter. This difference is reflected in the lower maximum load reached by the PW carbon specimen, as the resin content is a factor affecting the strength of the laminate. Both types of specimens showed fibre wrinkling in the upper area, just below the loading nose. Interestingly, there was a clear, acute fibre breakage at the bottom. The fibre fracture mainly affected bundles in the horizontal direction, perpendicular to the load path, while those in the vertical direction remained intact. The bundles in the horizontal direction appeared almost undeformed, in contrast to the split bundles in the vertical direction, due to the lower strength of the matrix compared to that of the fibres.

Fig. 8 illustrates the micrographs of the fracture surfaces of the aramid samples. Similar to the carbon specimens, aramid specimens also showed fibre wrinkling in the upper region, just below the loading nose, and fibre tensile failure in the bottom zone. Also in this case, only horizontal fibres were broken by tensile stress, showing signs of fibre fraying, contrary to the damaged surface of the carbon laminate, that looked clean and brittle. Contrary to the all-titanium specimen, crack propagation followed a straight path along a vertical bundle. The reinforcing fibres fractured brittlely, tearing after being ejected from the matrix by the applied tensile stress. The shear force transmitted by the three-point bending stress caused the reinforcing fibres to bend, leading to the collapse of the matrix element and misaligning the reinforcing fibres. However, the fibre strands did not become entangled as a result.

It is worth making a comparison with data inherent in the out of plane bending loading, carried out in a previous work by the same authors [29]. In that case, the CFRP specimens were found to possess higher flexural strength compared to AFRP. In fact, there was an increase in the maximum load and performance index of 47.6% and 43.0%, respectively. The difference in the performance index was lower because the aramid fibre composite is lighter. In the case analysed in the present article, the TW carbon specimens presented an increase, compared to aramid skin specimens, in the maximum load and the performance index of 11.6% and 8.5%, respectively. On the contrary, the PW carbon samples presented a decrease, compared to the aramid ones, in the maximum load and the performance index of 21.6% and 7.0%, respectively. Different damage mechanisms were identified for the two skin materials, similar to those found in the present study, even if the loading conditions were dissimilar. In fact, the carbon fibre skins presented a sharp fracture surface, while the aramid fibre ones showed fraying, as shown in Fig. 9. This difference was reflected in the shape of the load-displacement curve, which in the former case presented a clear load drop after a linear load increase, while in the latter, the curve reached an almost horizontal asymptote before failure.

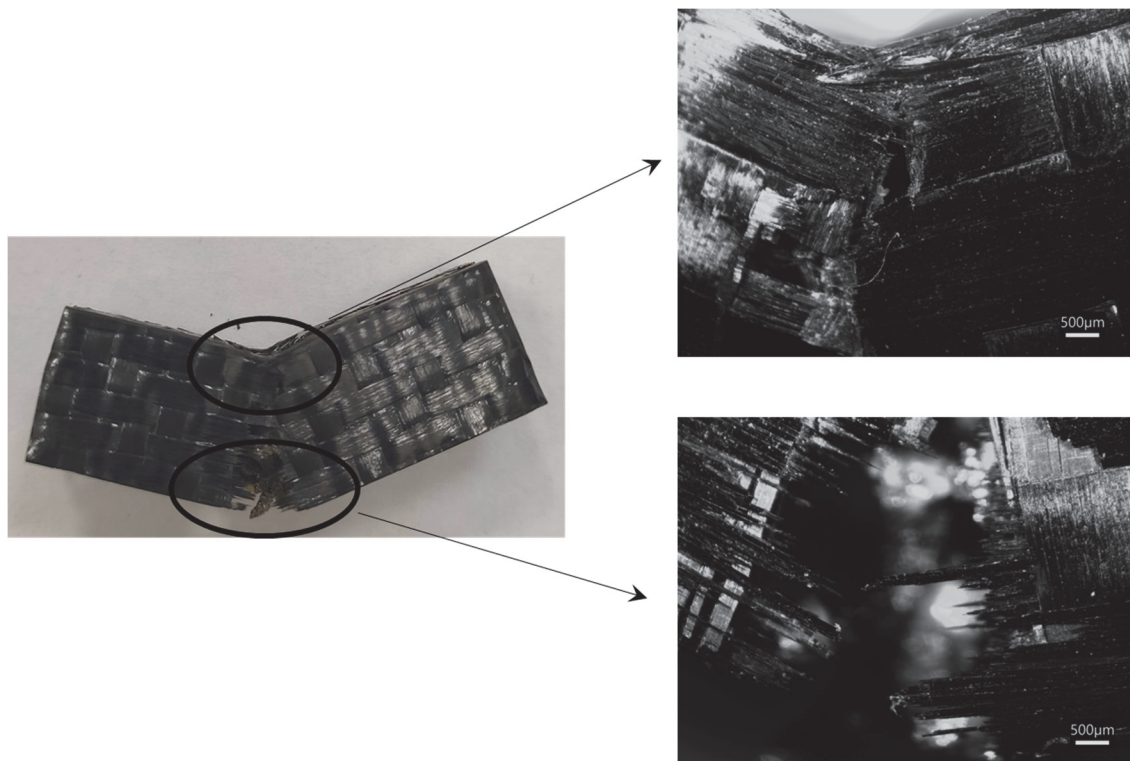


Figure 6: TW carbon-skin fractured specimen.

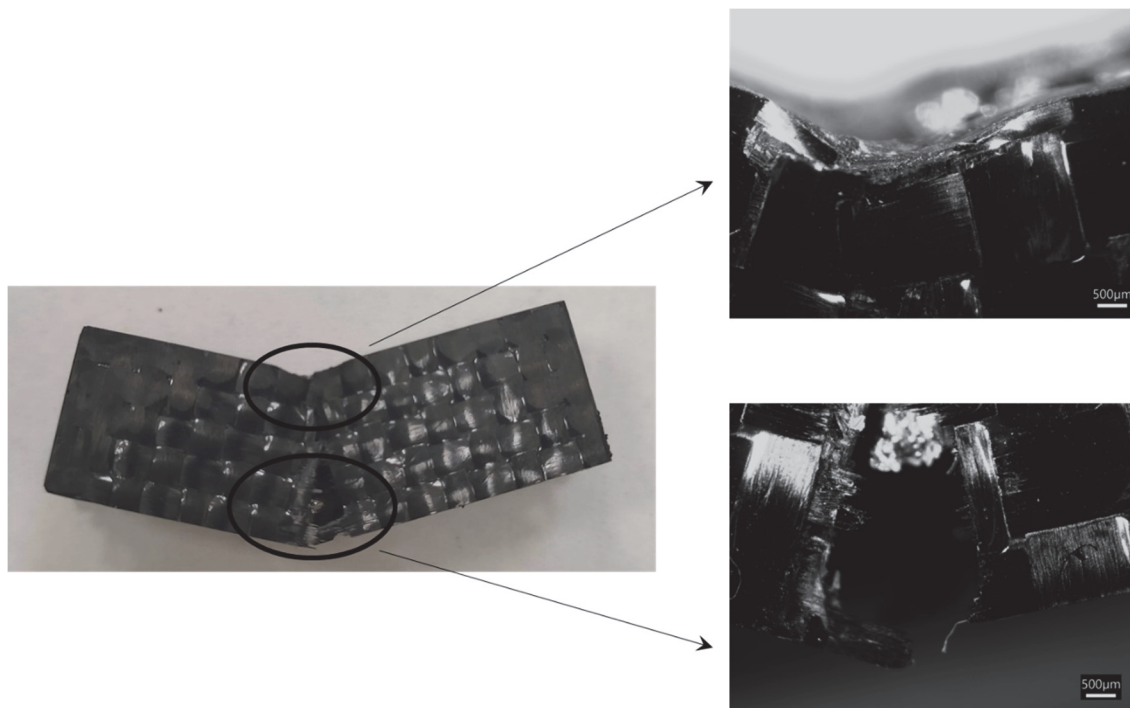


Figure 7: PW carbon-skin fractured specimen.

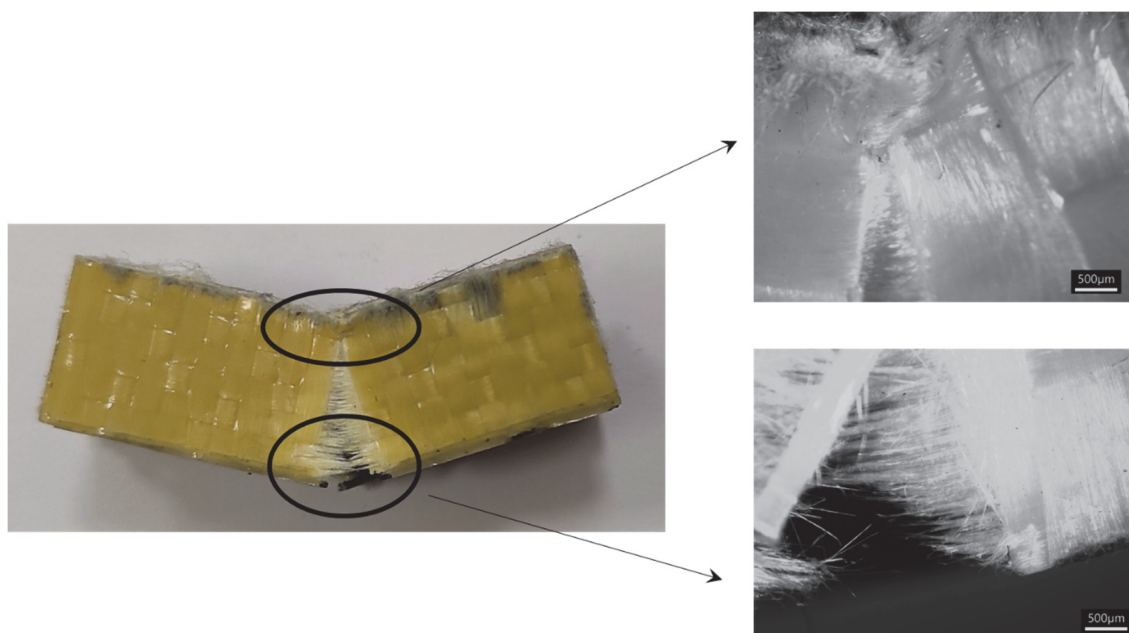


Figure 8: Aramid-skin fractured specimen.

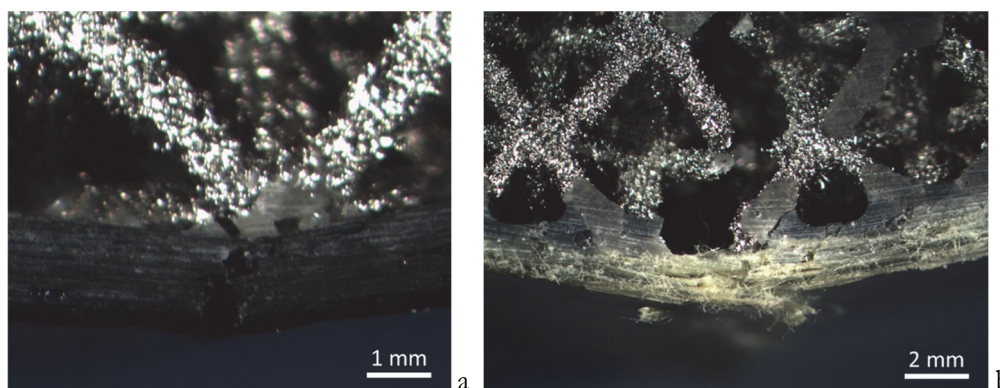


Figure 9: Surface fracture of out-of-plane bending loaded specimens: a) carbon fibre skin, b) aramid fibre skin.

CONCLUSIONS

In the present work, the study on the in-plane flexural behaviour of various FRP (Fibre Reinforced Polymer)-titanium hybrid specimens were presented. Specifically, three types of FRP skins were considered, with a titanium alloy core that consisted in a lattice structure. In particular, the study examined two different types of CFRP (Carbon Fibre Reinforced Polymer): one presenting a plain weave style, the other characterized by a twill weave style. The third type of composite material was an AFRP (Aramid Fibre Reinforced Polymer). Moreover, a fourth type of specimen was considered, that presented both core and skins made of titanium. As concerns the manufacturing process, the hybrid specimens were produced in a two-steps process: first, the lattice cores were created using the additive manufacturing process known as EBM (Electron Beam Melting), then the skins were added using autoclave vacuum bagging, where the skins were cured directly on the core, that acted as a mould. As concerns the all-titanium samples, both core and skins were produced in a single run through the EBM (single-step process).

Even though the aramid structure showed a larger residual load capacity, the experimental testing campaign showed relatively comparable mechanical characteristics for AFRP (Aramid Fibre Reinforced Polymer) and CFRP (Carbon Fibre Reinforced Polymer) specimens, with an equivalent load-displacement pattern. On the contrary, the specimen with titanium skin presented a higher load to failure. However, the performance index parameter was introduced to take into consideration



also the weight, that is a point of strength of composite material. In fact, by considering the maximum load alone, in the case of the TW carbon skin specimens, there was a reduction of 38% compared to the titanium skin specimens. This difference rose to 45% and 46% for those with the aramid composite and PW carbon skins, respectively. As for the performance index, a reduction of just 5% is observed for TW carbon specimens, while for aramid and PW carbon specimens it was 13% and 18%, respectively. For the latter two materials, the difference is more pronounced than in the case of the maximum load alone because the density of aramid is lower.

In terms of the fracture surface analysis, it should be noted that the titanium skin presented a quite irregular crack path, that followed the boundary of partially melted powder particles. Moreover, the appearance of the fracture surface denoted a ductile failure mechanism. As for the FRP samples, distinct damage mechanisms were observed for the fibres that failed in the area subjected to tensile stress: a fraying was found for the aramid fibres, whereas a sharp fracture was seen in the carbon fibre specimens.

ACKNOWLEDGEMENTS

This research was supported by POR FESR Lazio 2014-2020, Strategic Projects-AoS Aerospace [AMHybridStructures project, 28143, rif. G06734/2020].

REFERENCES

- [1] Amin Yavari, S., Ahmadi, S.M., Wauthle, R., Pouran, B., Schrooten, J., Weinans, H., Zadpoor, A.A. (2015). Relationship between unit cell type and porosity and the fatigue behavior of selective laser melted meta-biomaterials, *J. Mech. Behav. Biomed. Mater.*, 43, pp. 91–100, DOI: 10.1016/j.jmbbm.2014.12.015.
- [2] Ashby, M.F. (2006). The properties of foams and lattices, *Philos. Trans. R. Soc. A Math. Phys. Eng. Sci.*, 364(1838), pp. 15–30, DOI: 10.1098/rsta.2005.1678.
- [3] Bellini, C., Borrelli, R., Di Cocco, V., Franchitti, S., Iacoviello, F., Mocanu, L.P., Sorrentino, L. (2021). Failure energy and stiffness of titanium lattice specimens produced by electron beam melting process, *Mater. Des. Process. Commun.*, pp. 1–6, DOI: 10.1002/mdp2.268.
- [4] Bellini, C., Borrelli, R., Di Cocco, V., Franchitti, S., Iacoviello, F., Sorrentino, L. (2022). Titanium lattice structures manufactured by EBM process: effect of skin material on bending characteristics, *Eng. Fract. Mech.*, 260, pp. 108180, DOI: 10.1016/j.engfracmech.2021.108180.
- [5] Fan, H.-L., Zeng, T., Fang, D.-N., Yang, W. (2010). Mechanics of advanced fiber reinforced lattice composites, *Acta Mech. Sin.*, 26(6), pp. 825–835, DOI: 10.1007/s10409-010-0390-z.
- [6] Bellini, C., Di Cocco, V., Iacoviello, F., Mocanu, L.P., Berto, F. (2024). Material choice to optimise the performance index of isogrid structures, *Frat. Ed Integrità Strutt.*, 18(67), pp. 231–239, DOI: 10.3221/IGF-ESIS.67.17.
- [7] Queheillalt, D.T., Murty, Y., Wadley, H.N.G. (2008). Mechanical properties of an extruded pyramidal lattice truss sandwich structure, *Scr. Mater.*, 58(1), pp. 76–79, DOI: 10.1016/j.scriptamat.2007.08.041.
- [8] Dong, G., Tang, Y., Zhao, Y.F. (2017). A survey of modeling of lattice structures fabricated by additive manufacturing, *J. Mech. Des. Trans. ASME*, 139(10), DOI: 10.1115/1.4037305.
- [9] Razavi, S.M.J., Avanzini, A., Cornacchia, G., Giorleo, L., Berto, F. (2021). Effect of heat treatment on fatigue behavior of as-built notched Co-Cr-Mo parts produced by Selective Laser Melting, *Int. J. Fatigue*, 142, pp. 105926, DOI: 10.1016/j.ijfatigue.2020.105926.
- [10] Benedetti, M., du Plessis, A., Ritchie, R.O., Dallago, M., Razavi, S.M.J., Berto, F. (2021). Architected cellular materials: A review on their mechanical properties towards fatigue-tolerant design and fabrication, *Mater. Sci. Eng. R Reports*, 144, pp. 100606, DOI: 10.1016/j.mser.2021.100606.
- [11] Bellini, C., Borrelli, R., Di Cocco, V., Franchitti, S., Iacoviello, F., Sorrentino, L. (2021). Damage analysis of Ti6Al4V lattice structures manufactured by electron beam melting process subjected to bending load, *Mater. Des. Process. Commun.*, (April), pp. 1–4, DOI: 10.1002/mdp2.223.
- [12] Leary, M., Mazur, M., Elambasseril, J., McMillan, M., Chirent, T., Sun, Y., Qian, M., Easton, M., Brandt, M. (2016). Selective laser melting (SLM) of AlSi12Mg lattice structures, *Mater. Des.*, 98, pp. 344–357, DOI: 10.1016/j.matdes.2016.02.127.
- [13] Lampeas, G., Diamantakos, I., Ptochos, E. (2019). Multifield modelling and failure prediction of cellular cores produced



- by selective laser melting, *Fatigue Fract. Eng. Mater. Struct.*, 42(7), pp. 1534–1547, DOI: 10.1111/ffe.13008.
- [14] Epasto, G., Palomba, G., D’Andrea, D., Guglielmino, E., Di Bella, S., Traina, F. (2019). Ti-6Al-4V ELI microlattice structures manufactured by electron beam melting: Effect of unit cell dimensions and morphology on mechanical behaviour, *Mater. Sci. Eng. A*, 753, pp. 31–41, DOI: 10.1016/j.msea.2019.03.014.
- [15] Liu, L., Kamm, P., García-Moreno, F., Banhart, J., Pasini, D. (2017). Elastic and failure response of imperfect three-dimensional metallic lattices: the role of geometric defects induced by Selective Laser Melting, *J. Mech. Phys. Solids*, 107, pp. 160–184, DOI: 10.1016/j.jmps.2017.07.003.
- [16] Mahbod, M., Asgari, M. (2019). Elastic and plastic characterization of a new developed additively manufactured functionally graded porous lattice structure: Analytical and numerical models, *Int. J. Mech. Sci.*, 155(February), pp. 248–266, DOI: 10.1016/j.ijmecsci.2019.02.041.
- [17] Cantaboni, F., Ginestra, P.S., Tocci, M., Avanzini, A., Ceretti, E., Pola, A. (2022). Compressive behavior of Co-Cr-Mo radially graded porous structures under as-built and heat-treated conditions, *Frat. Ed Integrita Strutt.*, 16(62), pp. 490–504, DOI: 10.3221/IGF-ESIS.62.33.
- [18] Magarò, P., Alaimo, G., Carraturo, M., Sgambitterra, E., Maletta, C. (2023). A novel methodology for the prediction of the stress–strain response of laser powder bed fusion lattice structure based on a multi-scale approach, *Mater. Sci. Eng. A*, 863(July 2022), pp. 144526, DOI: 10.1016/j.msea.2022.144526.
- [19] Carraturo, M., Alaimo, G., Marconi, S., Negrello, E., Sgambitterra, E., Maletta, C., Reali, A., Auricchio, F. (2021). Experimental and Numerical Evaluation of Mechanical Properties of 3D-Printed Stainless Steel 316L Lattice Structures, *J. Mater. Eng. Perform.*, 30(7), pp. 5247–5251, DOI: 10.1007/s11665-021-05737-w.
- [20] Bellini, C., Borrelli, R., Di Caprio, F., Di Cocco, V., Franchitti, S., Iacoviello, F., Pirozzi, C., Sorrentino, L. (2023). Geometrical Accuracy Analysis of Ti-6Al-4V Trusses Manufactured by Electron Beam Melting Process, *Metals (Basel)*, 13(8), DOI: 10.3390/met13081454.
- [21] Di Caprio, F., Franchitti, S., Borrelli, R., Bellini, C., Di Cocco, V., Sorrentino, L. (2022). Ti-6Al-4V Octet-Truss Lattice Structures under Bending Load Conditions : Numerical and Experimental Results, *Metals (Basel)*, 12, pp. 410.
- [22] Fiorentin, F.K., Oliveira, B., Pereira, J.C.R., Correia, J.A.F.O., de Jesus, A.M.P., Berto, F. (2021). Fatigue behaviour of metallic components obtained by topology optimization for additive manufacturing, *Frat. Ed Integrita Strutt.*, 15(55), pp. 119–135, DOI: 10.3221/IGF-ESIS.55.09.
- [23] Taghipoor, H., Damghani Nouri, M. (2020). Axial crushing and transverse bending responses of sandwich structures with lattice core, *J. Sandw. Struct. Mater.*, 22(3), pp. 109963621876132, DOI: 10.1177/1099636218761321.
- [24] Zargarian, A., Esfahanian, M., Kadkhodapour, J., Ziari-Rad, S., Zamani, D. (2019). On the fatigue behavior of additive manufactured lattice structures, *Theor. Appl. Fract. Mech.*, 100, pp. 225–232, DOI: 10.1016/j.tafmec.2019.01.012.
- [25] Figlus, T., Koziol, M., Kuczyński, Ł. (2019). The effect of selected operational factors on the vibroactivity of upper gearbox housings made of composite materials, *Sensors (Switzerland)*, 19(19), DOI: 10.3390/s19194240.
- [26] Koziol, M. (2019). Evaluation of classic and 3D glass fiber reinforced polymer laminates through circular support drop weight tests, *Compos. Part B Eng.*, 168(November 2018), pp. 561–571, DOI: 10.1016/j.compositesb.2019.03.078.
- [27] Taghipoor, H., Damghani Nouri, M. (2020). Axial crushing and transverse bending responses of sandwich structures with lattice core, *J. Sandw. Struct. Mater.*, 22(3), pp. 572–598, DOI: 10.1177/1099636218761321.
- [28] Zhang, J., Ding, S., Yanagimoto, J. (2022). Bending properties of sandwich sheets with metallic face sheets and additively manufactured 3D CFRP lattice cores, *J. Mater. Process. Technol.*, 300(November 2021), pp. 117437, DOI: 10.1016/j.jmatprotec.2021.117437.
- [29] Bellini, C., Borrelli, R., Di Caprio, F., Di Cocco, V., Franchitti, S., Iacoviello, F., Mocanu, L.P., Sorrentino, L. (2022). Hybrid structures in Titanium-Lattice/FRP: effect of skins material on bending characteristics, *Procedia Struct. Integr.*, 41, pp. 3–8, DOI: 10.1016/j.prostr.2022.05.002.